Conformation of ATP and ADP Bound to N^{10}-Formyltetrahydrofolate Synthetase Determined by TRNOE NMR Spectroscopy†

Sophie Song,‡ David Vander Velde,§ Christopher W. Gunn,∥ and Richard H. Himes*,‡

Department of Biochemistry, Nuclear Magnetic Resonance Laboratory, and Molecular Graphics Laboratory, University of Kansas, Lawrence, Kansas 66045

Received August 24, 1993; Revised Manuscript Received November 5, 1993⊛

ABSTRACT: ATP and ADP bind to N^{10}-CHO-H_4folate synthetase from *Clostridium cylindrosporum* at four identical sites. Although both ADP and ATP bind to the enzyme with essentially the same K_a values as the Mg^{2+}·nucleotide complexes, only the Mg^{2+}·nucleotides are kinetically active. Using transferred nuclear Overhauser effect (TRNOE) NMR spectroscopy, we have measured the time-dependent NOE buildup rates of selected protons in ADP and ATP bound to N^{10}-CHO-H_4folate synthetase after preirradiating protons H1′, H2′, H3′, and H4′. The results were used to calculate interproton distances. In order to define the conformations of ADP and ATP bound to the enzyme, we used the TRNOE distance constraints in a distance geometry algorithm. The results of the distance geometry calculations suggest that, within experimental error, the conformations of both ADP and ATP (with or without Mg^{2+}) have an average glycosidic torsion angle X (O4′–C1′–N9–C8) of 100° ± 20° and a sugar pucker angle Ψ′ (C5′–C4′–C3′–O3′) of 85° ± 5°. These values are consistent with a nucleotide structure generated by computer modeling after energy minimization, which has X = 90° ± 6° and Ψ′ = 81°, indicating a high-*anti* and C3′-*endo* conformation.

N^{10}-Formyltetrahydrofolate (N^{10}-CHO-H_4folate)[1] synthetase catalyzes the formylation of H_4folate according to eq 1. H_4Folate synthetase from *Clostridia* is a homotetramer

$$HCOO^- + MgATP^{2-} + H_4\text{folate} \rightleftharpoons N^{10}\text{-CHO-}H_4\text{folate} + MgADP^- + P_i^{2-} \quad (1)$$

with a molecular mass of 240 kDa. Each monomer contains one nucleotide binding site (Curthoys & Rabinowitz, 1971, 1972). Previous kinetic studies have shown that the kinetically active form of the nucleotide is a Mg^{2+}·nucleotide complex (Himes & Wilder, 1965), although ligand binding studies have shown that the free nucleotides bind to the enzyme with K_a values similar to those for the Mg^{2+} complexes (Curthoys & Rabinowitz, 1971; Curthoys et al., 1972). As part of our studies of the catalytic mechanism of this enzyme, we were interested in knowing and comparing the conformations of the bound forms of the Mg^{2+}-complexed and -uncomplexed nucleotides.

The transferred nuclear Overhauser effect (TRNOE) method is an effective way to determine the conformation of nucleotides bound to proteins (Clore & Gronenborn, 1983; Rosevear & Mildvan, 1989; Williams & Rosevear, 1991). In the present study, using a one-dimensional NMR technique, we have measured selective interproton TRNOE(s) of the nucleotides in the E·ADP and E·ATP complexes, each in the absence and presence of Mg^{2+}. Combining the calculated interproton distances from the time-dependent NOE buildup data with a distance geometry algorithm leads to the conclusion that, in solution, the conformations of the nucleotides in different complexes are identical, showing a high-*anti* glycosidic torsion angle (X = 100° ± 20°) and a C3′-*endo* sugar pucker angle (Ψ′ = 85° ± 5°).

EXPERIMENTAL PROCEDURES

Materials. N^{10}-CHO-H_4folate synthetase was purified from *Clostridium cylindrosporum* using the method described previously (Staben et al., 1987). *C. cylindrosporum* was provided by the Biochemical Research Service Laboratory, University of Kansas. The specific activity of various preparations of the enzyme ranged from 386 to 422 $\mu mol \cdot min^{-1} \cdot mg^{-1}$. D_2O (99.9% enriched) was obtained from Cambridge Isotope Laboratories. Bio-Gel A15m used in heparin–agarose chromatography was obtained from Bio-Rad Laboratories. TSP, the internal standard for NMR experiments, was obtained from Aldrich Chemical Co. P^1,P^5-Di(adenosine-5′) pentaphosphate (DAP), an adenylate kinase inhibitor, and other chemicals used in this study were obtained from Sigma Chemical Co.

Preparation of Samples for NMR Measurements. Purified N^{10}-CHO-H_4folate synthetase (about 4 mg), stored as a crystalline suspension in 60% $(NH_4)_2SO_4$, was collected by centrifugation, redissolved in 50 μL of D_2O (99.9%) buffer [100 mM $KHCO_3$ (pH 7.5)/10 mM K_2SO_4], and centrifuged through a 1-mL column of Sephadex G-25. To reduce the H_2O content, the sample was then concentrated by centrifugation using a Millipore Ultrafree-MC filter unit, and the final volume was brought to 0.5 mL by adding D_2O buffer. A typical sample used in NMR measurements contained 0.1 mM enzyme binding sites and either 1.5 mM ATP or 3 mM ADP plus 0.12 mM DAP. When included, the $MgCl_2$ concentration was 3 mM in the ATP experiments and 6 mM in the ADP experiments. About 90% of the enzyme activity was recovered after the NMR experiments. NMR sample

† This work was supported by National Institutes of Health Grant DK-07140 and the University of Kansas General Research Fund.

* Address correspondence to this author. Phone: (913) 864-3813. Fax: (913) 864-5321.

‡ Department of Biochemistry, University of Kansas.

§ Nuclear Magnetic Resonance Laboratory, University of Kansas.

∥ Molecular Graphics Laboratory, University of Kansas.

⊛ Abstract published in *Advance ACS Abstracts,* January 1, 1994.

[1] Abbreviations: N^{10}-CHO-H_4folate, N^{10}-formyltetrahydrofolate; TRNOE, transferred nuclear Overhauser effect; RP-HPLC, reversed-phase high-pressure liquid chromatography; DAP, P^1,P^5-di(adenosine-5′) pentaphosphate; TSP, 3-(trimethylsilyl)propionic acid, sodium salt; EDTA, ethylenediaminetetraacetic acid.

0006-2960/94/0433-693$04.50/0

tubes were previously stored overnight in 2 mM EDTA, rinsed thoroughly with deionized distilled water, and dried.

NMR Spectroscopy. Spectra were recorded on a Bruker AM-500 NMR spectrometer with an Aspect 3000 data system operating at 500.14 MHz for ^{1}H. A dedicated proton probe optimized for water suppression experiments was employed. Chemical shifts were referenced to TSP. All measurements were performed at 10 °C.

Selective T_1's were measured by the inversion–recovery method with a low-power $90°_x$–$180°_y$–$90°_x$ composite 180° pulse (ca. 50-Hz field strength) using 10 τ values between 0.15 and 5 T_1's. The relaxation times were calculated with a nonlinear three-parameter least-squares fit to the intensity of the inverted peak. TRNOE buildup curves were measured by a series of seven 1D NOE difference experiments with irradiation periods varying from 25 to 200 ms. The sum of the irradiation period and the preacquisition delay was held constant at 2 s. For each irradiation time, 32 acquisitions followed 4 dummy scans at each frequency, with 10 cycles through the frequency list (corresponding to the frequencies of H1′, H2′, H3′, and H4′ plus two blanks at 10.5 and −1 ppm which were far from any peaks of interest). NOE's were calculated from the resulting difference spectra. The difference spectrum showing the fewest subtraction artifacts was used in every case.

The residual water signal in the samples was substantially larger than the signals of interest, so it was suppressed by presaturation. Since the relaxation and NOE experiments require low-power pulses, typically from the decoupler, simultaneous water presaturation was accomplished using a second channel derived from the gated low-power output of the transmitter (ordinarily used for decoupling in inverse-mode experiments). The power level of the second channel was controlled with a precision RF attenuator. The second channel, which is necessarily at the carrier frequency, was used for selective inversion in the T_1 experiments and water suppression in the NOE measurements in order to take best advantage of the phase coherence of this channel with the high-power pulses observed.

T_2 measurements were performed with the Carr–Purcell–Meiboom–Gill (CPMG) sequence adapted for water presaturation (Meiboom & Gill, 1958). The sequence provided by Bruker gave satisfactory results down to a τ delay of approximately 1 ms; shorter values exceeded the duty cycle limitations of the transmitter, and an inverse-mode experiment employing the decoupler as the proton transmitter was required to obtain the spectra.

Calculation of Cross-Relaxation Rates and Interproton Distances. Using a two-spin approximation and an assumption of a single correlation time of the macromolecule, cross-relaxation rates (σ_{AB}) and interproton distances can be calculated from the time dependence of NOE's [$f_A(B)_t$] and selective longitudinal relaxation rates (ρ_A) as described previously (Rosevear & Mildvan, 1989). For instantaneous saturation of spin B (corrections for noninstantaneous saturation were found to be negligible for our data), the time dependence of the NOE observed at spin A is given by

$$f_A(B)_t = \sigma_{AB}/\rho_A(1 - e^{-\rho_A t}) \quad (2)$$

where the selective relaxation rate ρ_A is independently determined in the selective inversion–recovery experiment. NOE buildup curves were fitted using the program MINSQ (Micro Math Scientific Software, Salt Lake City, UT). The cross-relaxation rate σ_{AB} determined from the fit is proportional to the sixth root of the interproton distance; the distances were calculated by scaling to the observed cross-relaxation rate for H1′ and H2′. The distance between H1′ and H2′ was assumed to be fixed at 2.9 ± 0.2 Å (Williams & Rosevear, 1991). The experimentally determined distances were assumed to be subject to an additional 10% uncertainty for distance geometry calculations. Distance geometry calculations (Kuntz et al., 1989) were performed with DSpace 4.0 (Hare Research, Bothell, WA) on a Silicon Graphics Indigo computer.

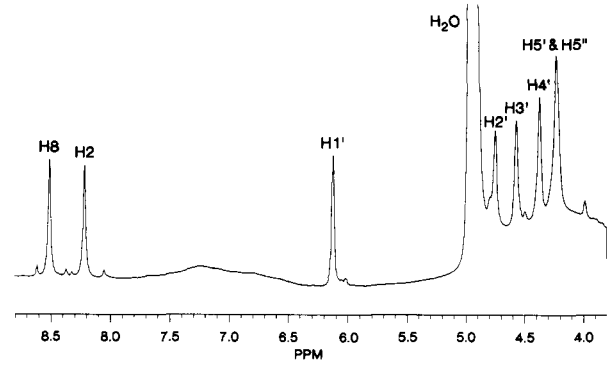

FIGURE 1: ^{1}H-NMR spectrum of ADP in the presence of enzyme. The mixture contained 3 mM ADP, 6 mM Mg^{2+}, and 0.1 mM enzyme sites. The spectrum was obtained by preirradiating at 10.5 ppm for 100 ms. The protons of interest are identified.

Model Building. Energetics of variations of the glycosidic angle X (torsion defined by O4′–C1′–N9–C8) were explored using Sybyl 5.5 (Tripos Associates, St. Louis, MO) on an IBM RS/6000 Model 560 workstation running AIX V3.2.0.0. The Tripos' Sybyl 5.2 force field (Clark et al., 1989) as enhanced for releases 5.3–5.5 (Tripos, 1992) was used for energy calculations. The electrostatic energy contributions of partial atomic charges were omitted ("ignore charges" option) to avoid the complexities involved in placement of counterions to reduce the strong effects of partial charges on the phosphate chain. The technique used for conformational analysis was the Sybyl "gridsearch," in which the torsion angle X under investigation was rotated to a series of predefined values, at each step of which the geometries of all other parts of the molecule were optimized to a local energy minimum, using the Sybyl "maximin" minimizer.

Other Methods. Protein concentration was determined by using the method of Bradford (1976) or an extinction coefficient of 1.22×10^5 $M^{-1}\cdot cm^{-1}$ (Himes & Cohn, 1967). The enzyme activity was assayed as previously described (Rabinowitz & Pricer, 1962). By using RP-HPLC for nucleotide analysis, we observed a very low level of contamination by adenylate kinase which over the long time period of the NMR measurements (24 h or more) in the ADP experiments would have converted ADP to a significant amount of ATP. This action was inhibited by the addition of the adenylate kinase inhibitor DAP (0.12 mM).

RESULTS AND DISCUSSION

Time-Dependent NOE Buildups. To calculate the cross-relaxation rates (σ_{AB}), we measured the time-dependent TRNOE's in the various enzyme–nucleotide complexes. Figure 1 shows a region of the control NMR spectrum of a solution of the enzyme·Mg^{2+}·ADP complex obtained by preirradiating at 10.5 ppm for 100 ms. In this spectrum, from downfield to upfield, adenine H8 and H2 and H1′, H2′, H3′, and H4′ protons could be easily identified. The NOE difference spectrum was generated by subtracting the control

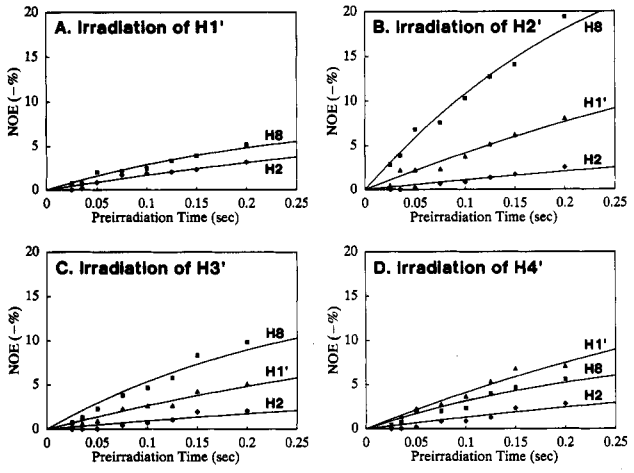

FIGURE 2: Time-dependent NOE buildup for adenosine protons of Mg^{2+}·ADP bound to N^{10}-CHO-H_4folate synthetase. (A) NOE buildup of adenine H8 and H2 upon preirradiation of ribose H1′. (B) NOE buildup of adenine H8, ribose H1′, and adenine H2 upon preirradiation of ribose H2′. (C) NOE buildup of adenine H8, ribose H1′, and adenine H2 upon preirradiation of ribose H3′. (D) NOE buildup of adenine H8, ribose H1′, and adenine H2 upon preirradiation of ribose H4′. Conditions are described under Experimental Procedures.

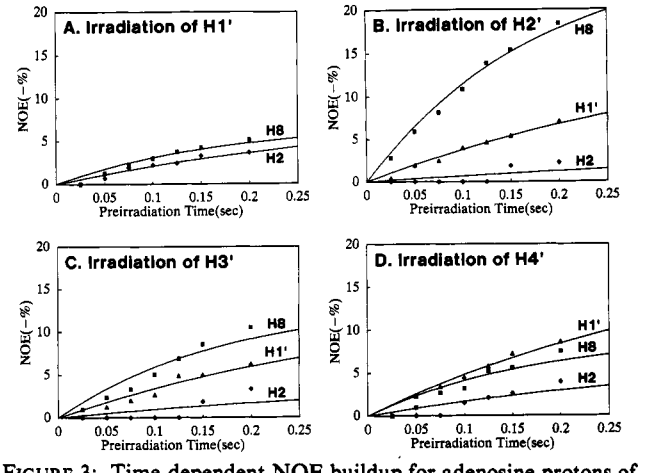

FIGURE 3: Time-dependent NOE buildup for adenosine protons of Mg^{2+}·ATP bound to N^{10}-CHO-H_4folate synthetase. (A) NOE buildup of adenine H8 and H2 upon preirradiation of ribose H1′. (B) NOE buildup of adenine H8, ribose H1′, and adenine H2 upon preirradiation of ribose H2′. (C) NOE buildup of adenine H8, ribose H1′, and adenine H2 upon preirradiation of ribose H3′. (D) NOE buildup of adenine H8, ribose H1′, and adenine H2 upon preirradiation of ribose H4′. Conditions are described under Experimental Procedures.

spectrum from the experimental spectrum which was collected after preirradiating a selected proton. The magnitudes of the NOE in the difference spectra were determined by peak height measurement. Since the peaks in the NOE difference spectra appear as negative values, the magnitude of the NOE was calculated as the negative percentage of the corresponding magnitude in the control spectrum.

Figure 2 presents the time-dependent NOE buildups of selected protons after irradiation of H1′, H2′, H3′, and H4′ in the enzyme·Mg^{2+}·ADP complex. It is important to distinguish primary NOE effects (those originating from short internuclear distances in the bound state, which are visible at early times in the buildup curve) from the secondary effects likely arising from spin diffusion. Preirradiation of H1′ (Figure 2A) caused no primary NOE's on either adenine H8 or adenine H2. Less than 2.5% NOE was observed at these protons after 100 ms. On the other hand, preirradiation of H2′ (Figure 2B) induced primary NOE's on adenine H8. The NOE buildup was 10% within 100 ms. Preirradiation of H2′ did not produce primary NOE's at adenine H2. Preirradiation of H3′ generated primary NOE's at adenine H8, but not at adenine H2 (Figure 2C). Finally, preirradiation of H4′ caused primary NOE's at H1′ (Figure 2D), but not at adenine H2. Figure 3 presents the time-dependent NOE buildups of selected protons after irradiation of H1′, H2′, H3′, and H4′ in the enzyme·Mg^{2+}·ATP complex. The results were quite similar to those obtained in the enzyme·Mg^{2+}·ADP complex. In addition, results from the complexes in the absence of Mg^{2+} were indistinguishable from those containing Mg^{2+} (data not shown).

Exchange Rate and Nonspecific Binding Considerations. Recently the subject of small-molecule exchange rates, and the impact of finite rates on the accuracy of bound-state structures determined by the transferred NOE method, has received considerable attention in the literature (London et al., 1992; Glaudemans et al., 1990; Bevilacqua et al., 1990; Kohda et al., 1987). In this system, there does not appear to be any chemical shift change exceeding 0.01 ppm for ADP on binding, on the basis of titration data between 2:1 (approximately the minimum concentration at which the ADP signals can be located in the envelope of protein signals) and 30:1 ADP:enzyme site ratios. The absence of a chemical shift change on binding precludes a determination of the exchange rate from the dependence of the apparent T_2 on the length of the τ delay in a Carr–Purcell sequence, which has been successful in some cases (London et al., 1992; Gerig & Stock, 1975). However, even in the limit of no shift change, the change in T_2 as a function of the ligand:enzyme ratio can be used to set at least a lower bound on the exchange rate assuming eq 3 holds,as is likely in this system (Gerig & Stock, 1975),

$$T_2^{-1} = T_{2A}^{-1} + (X_B/X_A)(T_{2B} + \tau_B)^{-1} \quad (3)$$

where A and B denote free and bound sites, respectively, X is the mole fraction, and τ_B is the residence time in the bound state. The T_2 of the H8 and H2 ADP signals at 3 mM ADP/0.1 mM enzyme sites was determined by a CPMG experiment to be 77 ms, in excellent agreement with the measured line width of 4.0 Hz for these signals (chosen because they are singlets). Assuming the broader line widths observed at lower concentration ratios also reasonably reflect the T_2 under those conditions, the value of $(T_{2B} + \tau_B)^{-1}$ can be obtained from a plot of (Σ·line width) vs X_B [calculated from the concentrations used assuming a K_d of 100 μM (Curthoys & Rabinowitz, 1971)]. These plots were linear (data not shown) and had slopes of 140 s^{-1} for H2 and 250 s^{-1} for H8. Since T_{2B} can of course be different for the two sites, but τ_B must be the same, the higher value sets an absolute lower bound on the ADP off rate. The actual value is of course higher, because T_{2B} is not zero; from the K_d, it can be estimated to be around 10^4 assuming an association rate constant near the diffusion-controlled limit. These high off rates should not be a limiting factor in the accuracy of the bound-state distances determined in this study.

Particularly for multiply charged molecules such as nucleotides, another potential source of error in the transferred NOE experiment is significant electrostatic nonspecific binding to charged sites on the protein. Although the severity of such effects would be expected to depend strongly on the protein, it appears some proteins may nonspecifically bind nucleotides with K_d values in the millimolar range (Murali et al., 1993). Since a proteiin can potentially have several such sites, in

Table 1: Relaxation Rates for Selected Protons

protons	ρ_A (s^{-1})			
	E·Mg^{2+}·ADP	E·ADP	E·Mg^{2+}·ATP	E·ATP
H8	3.99	3.57	5.82	4.02
H2	1.47	1.48	2.71	2.03
H1′	1.88	1.68	2.79	2.03
H2′	4.48	3.76	4.31	4.27
H3′	3.74	2.88	4.93	3.61
H4′	2.72	2.69	3.92	3.21

unfavorable cases the amount of nucleotide bound nonspecifically could substantially exceed the amount bound specifically, and the off rates from the nonspecific sites could be much higher. Nonspecific binding could then dominate the observed TRNOE's. However, the nonspecific binding might be quite insensitive to nucleotide conformation; in this case, it could partially or totally obscure information about the conformational preferences of the active site. The high concentrations of ligand (and enzyme) favored in transferred NOE experiments (Campbell & Sykes, 1991) will tend to compound this problem. In order to assess the likelihood of nonspecific binding affecting the results of these experiments, another experiment near the lowest workable concentrations for the protocol employed here (1 mM ADP, 0.2 mM binding sites) was performed. These conditions could be sufficiently different from those employed earlier to alter the ratios of the specifically bound and putative nonspecifically bound nucleotides by an observable amount, under the assumptions listed above. Although the resulting buildup curves contained more scatter, the distance ratios derived from them were essentially identical to those obtained earlier. We believe nonspecific binding is consequently not introducing significant error in our results; it is worth noting that all the experiments reported here were done at nucleotide and enzyme concentrations that are relatively low compared to many TRNOE studies previously reported in the literature [e.g., see Rosevear et al. (1987)].

Interproton Distances and Distance Geometry. Using the inversion–recovery method as described under Experimental Procedures, the selective T_1's were measured. The selective longitudinal relaxation rates (ρ_A) calculated from $1/T_1$ are shown in Table 1. The ρ_A values obtained with the enzyme–nucleotide complexes in the presence of Mg^{2+} appeared to be slightly higher than the corresponding values in the complexes which did not contain Mg^{2+}. The results from both selective ρ_A's and the time-dependent NOE buildups were used to calculate the cross-relaxation rates (σ_{AB}) by using the MINSQ fitting program. The cross-relaxation rates (σ_{AB}) were then used to calculate the interproton distances under a two-spin approximation and an assumption of a single correlation time of the macromolecule, as described under Experimental Procedures. The results of cross-relaxation rates (σ_{AB}) and the calculated interproton distances (r_{AB}) are listed in Table 2.

Both qualitative evaluation of the NOE buildup curves (Figures 2 and 3) and quantitative calculation of the interproton distances suggest the closest distance is between adenine H8 and H2′. Also, there are short distances between adenine H8 and H3′, as well as between H1′ and H4′. The similar feature of the NOE buildups and the similar values of the interproton distances which were shared by the four different enzyme–nucleotide complexes (Figures 2 and 3; Table 2) reflect the conformation of the enzyme–bound ADP and ATP with an *anti* glycosidic torsion angle; the possibility of a *syn* glycosidic torsion angle is basically ruled out (Rosevear et al., 1983; Williams & Rosevear, 1991).

To define further the conformation of the enzyme-bound ADP and ATP, the distances listed in Table 2 were taken as constraints for distance geometry calculations in the Dspace 4.0 program, taking the uncertainty in the reference distance H1′–H2′ as ±0.2 Å, propagating this uncertainty through the experimental distance calculations, and adding an additional ±10% uncertainty (the final r_{AB} values used in the distance geometry algorithm are indicated as "bounds" in Table 2) to reflect errors in the experimentally determined parameters. The adenine H2 proton showed no NOE to any of the sugar protons at early measuring times, but small NOE's appeared after 100 ms. Because these are likely due to spin diffusion, cross-relaxation rates were not calculated. Only a lower bound distance of 3.5 Å was used for adenine H2 to H1′, H2′, H3′, and H4′ with no upper bound. After embedding of the bounds matrix in the Dspace program, 100 trial structures were generated by cycles of annealing and energy minimization. The X (O4′–C1′–N9–C8) and Ψ′ (C5′–C4′–C3′–O3′) angles measured from these structures are shown in Figures 4A and 5A, respectively. The X and Ψ′ angles measured from another 100 structures which were generated without any experimental distance constraints are shown in Figures 4B and 5B, respectively. Without the experimental constraints, the angles were sampled throughout the allowed ranges (Figures 4B and 5B). On the other hand, with the constraints, the glycosidic torsion angle X was in the high-*anti* range (100° ± 20°), and the sugar pucker Ψ′ was C3′-*endo* (85° ± 5°).

Previous data from X-ray studies have suggested that C3′-*endo* and C2′-*endo* are the sugar pucker conformations which usually occur in nucleotides (Altona & Sundaralingam, 1972). It has also been shown that the relative energy of the furanose ring falls to a minimum when the sugar pucker angle Ψ′ is around 80° (C3′-*endo*) (Levitt & Warshel, 1978). [This angle is given the designation δ in some publications (Rosevear & Mildvan, 1989)]. Therefore, the experimentally derived sugar pucker angle Ψ (85° ± 5°), by itself, is an energetically favorable conformation of the furanose ring.

Model Building. To provide evidence that the experimentally deduced conformation of the enzyme-bound nucleotide falls into a reasonable energy range, we utilized the computer model building method. Using the Sybyl 5.5 "gridsearch", we analyzed the energies of four different conformations

Table 2: Cross-Relaxation Rates and Interproton Distances in Various Complexes[a]

protons	σ_{AB} (s^{-1})		r_{AB} (Å)		σ_{AB} (s^{-1})		r_{AB} (Å)		bounds (Å)
	E·Mg^{2+}·ADP	E·ADP	E·Mg^{2+}·ADP	E·ADP	E·Mg^{2+}·ATP	E·ATP	E·Mg^{2+}·ATP	E·ATP	
H8–H1′	0.35	0.29	3.1	3.0	0.41	0.25	3.0	3.1	2.7–3.5
H8–H2′	1.31	1.33	2.5	2.3	1.51	1.28	2.4	2.4	2.1–3.0
H8–H3′	0.65	0.50	2.8	2.8	0.78	0.46	2.7	2.8	2.4–3.3
H8–H4′	0.38	0.28	3.0	3.0	0.54	0.28	2.8	3.0	2.4–3.5
H1′–H2′	0.46	0.36	2.9	2.9	0.44	0.37	2.9	2.9	2.7–3.1
H1′–H3′	0.29	0.20	3.2	3.2	0.39	0.23	3.0	3.1	2.7–3.7
H1′–H4′	0.45	0.34	2.9	2.9	0.55	0.33	2.8	2.9	2.5–3.3

[a] Relaxation rates are subject to ±10‰ error.

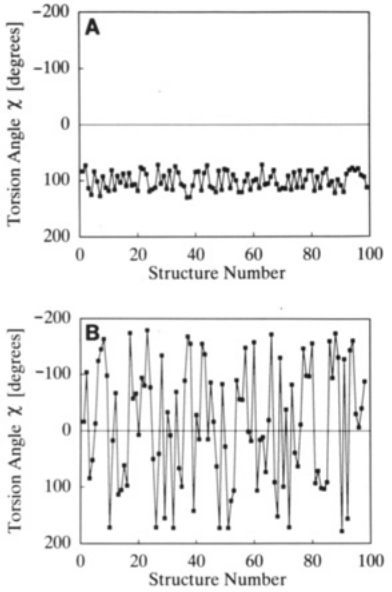

FIGURE 4: Distribution of the glycosidic torsion angle X generated from the Dspace distance geometry algorithm with or without experimental distance constraints. (A) Distribution of X with the experimental distance constraints using data from Table 2. (B) Distribution of X without any experimental distance constraints.

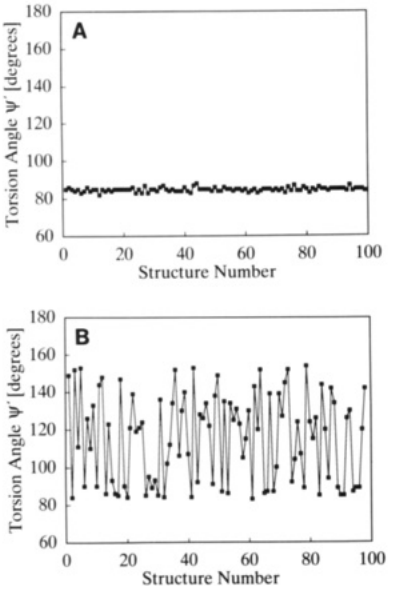

FIGURE 5: Distribution of the sugar pucker Ψ′ generated from the Dspace distance geometry algorithm with or without experimental distance constraints. (A) Distribution of Ψ′ with the experimental distance constraints using data from Table 2. (B) Distribution of Ψ′ without any experimental distance constraints.

generally adopted by free nucleotide in solution and compared them with the energy of the experimentally deduced conformation (Figure 6). For all conformational searches, the underlyiing starting conformation of the furanose ring was C3′-*endo*, with a sugar pucker angle Ψ′ at 80.7°, in a local energy minimum of 46.6 kcal/mol; X was 102.6° in this conformation. Three "gridsearch" runs were made with X rotated through all 360° in 3° increments. Two techniques were used: "original conformation" gridsearch and "continuous" gridseach. In "original conformation" gridsearch, X was successively set to each of 120 values (0, 3, 6, ..., 357°) with the remainder of the molecule being left in its initially-defined conformation; thus, the subsequent optimization of all geometries except X began with all such other geometries at the same point. In each of the two "continuous" gradsearch

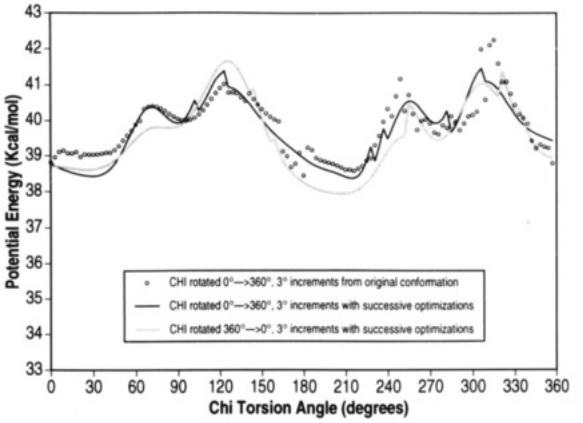

FIGURE 6: Energetics of a conformational search of the glycosidic torsion angle X in ADP and ATP bound to N^{10}-CHO-H$_4$folate synthetase.

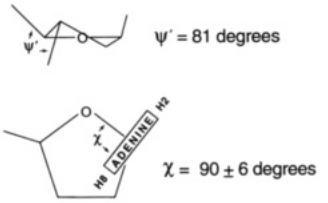

FIGURE 7: Conformation of ADP and ATP bound to N^{10}-CHO-H$_4$folate synthetase obtained from the distance geometry search and model building results.

runs, X was rotated to 120 values (0, 3, 6, ..., 357° as one direction, and 357, 354, ..., 0° as another direction) with run N starting from the optimized geometry of run N – 1. As in the "original" gridsearch, all geometries except X were allowed to optimize. The "original" gridsearch thus sampled the conformational range without respect to how the molecule reached each conformation; the "continuous" gridsearch simulated actual rotation of X in an adaptive sense.

Run A-original and Run B-continuous (which had positive rotation from 0 to 357°) found a distinct local minimum with X in a high-*anti* conformation (in a range of 90–96°), at approximately 1.5 kcal/mol above the global minimum (at which X was in the *syn* position, in the range of 180–210°). Local barriers about the high-*anti* local minimum were approximately 0.5 kcal/mol in the direction of a lower X and between 0.7 and 1.5 kcal/mol in the direction of a higher X. Run C-continuous (which had negative rotation from 357 to 0°) found an energy plateau for X values of 72–90° in which energies varied ±0.02 kcal/mol. There was essentially no local energy barrier in the direction of a lower X, and one of approximately 1.9 kcal/mol in the direction of a higher X. We therefore conclude that a nucleotide conformation characterized by a high-*anti*, C3′-*endo* conformation (X = 90° ± 6°, Ψ′ = approximately 81°) is a relatively low-energy local minimum and, from a molecular modeling standpoint, is a plausibly stable conformation. A representative of this conformation is presented in Figure 7.

In summary, by using the 1D TRNOE technique, we have defined the conformation of ADP and ATP bound to N^{10}-CHO-H$_4$folate synthetase. With or without Mg^{2+}, the conformations of the enzyme-bound ADP and ATP, showing a high-*anti* and C3′-*endo* conformation, are energetically acceptable. The *anti* conformation is commonly found in purine nucleotide binding proteins (Rosevear & Mildvan, 1989) although the *syn* conformation of ITP binds to aspartate transcarbamoylase (Banerjee et al., 1985). Further, because ADP and ATP and their Mg^{2+} complexes have the same

conformations, it is unlikely that the phosphate side chain interacts with the purine ring.

ACKNOWLEDGMENT

We thank B. D. Nagesewara Rao and N. Murali, IUPUI, for helpful discussions and communicating their results to us prior to publication.

REFERENCES

Altona, C., & Sundaralingam, M. (1972) *J. Am. Chem. Soc. 94*, 8205–8212.

Banerjee, A., Levy, H. R., Levy, G. C., & Chan, W. W.-C. (1985) *Biochemistry 24*, 1593–1598.

Bevilacqua, V. L., Thomson, D. S., & Prestegard, J. H. (1990) *Biochemistry 29*, 5529–5537.

Bradford, M. M. (1976) *Anal. Biochem. 72*, 248–254.

Campbell, A. P., & Sykes, B. D. (1991) *J. Magn. Reson. 93*, 77–92.

Clark, M., Cramer, R. D., & Van Opdenbosch, N. (1989) *J. Comput. Chem. 10*, 982–1012.

Clore, G. M., & Gronenborn, A. M. (1983) *J. Magn. Reson. 53*, 423–442.

Curthoys, N. P., & Rabinowitz, J. C. (1971) *J. Biol. Chem. 246*, 6942–6952.

Curthoys, N. P., D'Ari Straus, L., & Rabinowitz, J. C. (1972) *Biochemistry 11*, 345–349.

Gerig, J. T., & Stock, A. D. (1975) *Org. Magn. Reson. 7*, 249–255.

Glaudemans, C. P. J., Lerner, L., Daves, G. D., Kováč, P., Venable, R., & Bax, A. (1990) *Biochemistry 29*, 10906–10911.

Himes, R. H., & Wilder, T. (1965) *Biochim. Biophys. Acta 99*, 464–475.

Himes, R. H., & Cohn, M. (1967) *J. Biol. Chem. 242*, 3628–3635.

Kohda, D., Kawai, G., Yokoyama, S., Kawakami, M., Mizushima, S., & Miyazawa, T. (1987) *Biochemistry 26*, 6531–6538.

Kuntz, I. D., Thomason, J. F., & Oshiro, C. M. (1989) *Methods Enzymol. 177*, 159–204.

Levitt, M., & Warshel, A. (1978) *J. Am. Chem. Soc. 100*, 2607–2613.

London, R. E., Perlman, M. E., & Davis, D. G. (1992) *J. Magn. Reson. 97*, 79–98.

Meiboom, S., & Gill, D. (1958) *Rev. Sci. Instrum. 29*, 688–691.

Murali, N., Jarori, G. K., Landy, S. B., & Rao, B. D. N. (1993) *Biochemistry 32*, 12941–12948.

Rabinowitz, J. C., & Pricer, W. E., Jr. (1962) *J. Biol. Chem. 237*, 2898–2902.

Rosevear, P. R., & Mildvan, A. S. (1989) *Methods Enzymol. 177*, 333–358.

Rosevear, P. R., Bramson, H. N., O'Brian, C., Kaiser, E. T., & Mildvan, A. S. (1983) *Biochemistry 22*, 3439–3447.

Rosevear, P. R., Powers, V. M., Dowhan, D., Mildvan, A. S., & Kenyon, G. L. (1987) *Biochemistry 26*, 5338–5344.

Staben, C., Whitehead, T. R., & Rabinowitz, J. C. (1987) *Anal. Biochem. 162*, 257–264.

Williams, J. S., & Rosevear, P. R. (1991) *J. Biol. Chem. 266*, 2089–2098.